doi:10.1093/brain/awq212 Brain 2010: 133; 3423–3433 | 3423

BRAIN
A JOURNAL OF NEUROLOGY

Magnetic resonance imaging markers of Parkinson's disease nigrostriatal signature

Patrice Péran,[1,2] Andrea Cherubini,[1] Francesca Assogna,[3] Fabrizio Piras,[3] Carlo Quattrocchi,[1] Antonella Peppe,[3] Pierre Celsis,[2] Olivier Rascol,[2,4] Jean-François Démonet,[2] Alessandro Stefani,[5] Mariangela Pierantozzi,[5] Francesco Ernesto Pontieri,[6] Carlo Caltagirone,[3] Gianfranco Spalletta[3] and Umberto Sabatini[1]

1 Department of Radiology, I.R.C.C.S. Foundation Santa Lucia, Rome, Italy
2 INSERM U825, Université Paul-Sabatier, Toulouse, France
3 Laboratory of Clinical and Behavioural Neurology, IRCCS Santa Lucia Foundation, Rome, Italy
4 Clinical Investigation Centre (INSERM CIC-9302) and Department of Neurosciences, University Hospital and University of Toulouse, France
5 Department of Neuroscience, Tor Vergata University, Rome, Italy
6 Sapienza University, Second Faculty of Medicine, Department of Neurology, Rome, Italy

Correspondence to: Patrice Péran,
Department of Radiology,
I.R.C.C.S. Foundation Santa Lucia,
Via Ardeatina 306,
00179 Rome,
E-mail: p.peran@hsantalucia.it

One objective of modern neuroimaging is to identify markers that can aid in diagnosis, disease progression monitoring and long-term drug impact analysis. In this study, Parkinson-associated physiopathological modifications were characterized in six subcortical structures by simultaneously measuring quantitative magnetic resonance parameters sensitive to complementary tissue characteristics (i.e. volume atrophy, iron deposition and microstructural damage). Thirty patients with Parkinson's disease and 22 control subjects underwent 3-T magnetic resonance imaging with T_2*-weighted, whole-brain T_1-weighted and diffusion tensor imaging scans. The mean R_2* value, mean diffusivity and fractional anisotropy in the pallidum, putamen, caudate nucleus, thalamus, substantia nigra and red nucleus were compared between patients with Parkinson's disease and control subjects. Comparisons were also performed using voxel-based analysis of R_2*, mean diffusivity and fractional anisotropy maps to determine which subregion of the basal ganglia showed the greater difference for each parameter. Averages of each subregion were then used in a logistic regression analysis. Compared with control subjects, patients with Parkinson's disease displayed significantly higher R_2* values in the substantia nigra, lower fractional anisotropy values in the substantia nigra and thalamus, and higher mean diffusivity values in the thalamus. Voxel-based analyses confirmed these results and, in addition, showed a significant difference in the mean diffusivity in the striatum. The combination of three markers was sufficient to obtain a 95% global accuracy (area under the receiver operating characteristic curve) for discriminating patients with Parkinson's disease from controls. The markers comprising discriminating combinations were R_2* in the substantia nigra, fractional anisotropy in the substantia nigra and mean diffusivity in the putamen or caudate nucleus. Remarkably, the predictive markers involved the nigrostriatal structures that characterize Parkinson's physiopathology. Furthermore, highly discriminating combinations included markers from three different magnetic resonance parameters (R_2*, mean diffusivity and fractional anisotropy). These findings demonstrate that multimodal magnetic resonance imaging of subcortical grey matter structures is useful for the evaluation of Parkinson's disease and, possibly, of other subcortical pathologies.

Received March 30, 2010. Revised June 11, 2010. Accepted June 15, 2010. Advance Access publication August 23, 2010

Keywords: parkinsonism; iron; mean diffusivity; anisotropy; MRI

Abbreviations: DTI = diffusion tensor imaging; FLAIR = fluid-attenuated inversion recovery; LEDD = levodopa equivalent daily dose; ROC = receiver operating characteristic; UPDRS = Unified Parkinson's Disease Rating Scale

Introduction

The diagnosis of Parkinson's disease is based mainly on a set of clinical assessments that do not provide great accuracy (Hughes *et al.*, 1992; Caslake *et al*., 2008). Conventional MRI only aids in excluding underlying pathologies (e.g. vascular lesions). One objective of modern neuroimaging is to find markers that aid in diagnosis, disease progression monitoring and long-term drug impact evaluation. The main anatomical and functional changes induced by Parkinson's disease can be represented as a three-level system: mesencephalic (dopaminergic neuronal loss), basal ganglia (dopaminergic deafferentation) and cortical (functional reorganization) (Péran *et al*., 2006). Previous neuroimaging studies have generally focused on only one of these three levels. For example, nuclear medicine imaging techniques have been employed to assess the functional integrity of presynaptic nigrostriatal projections (for a review, see Pavese and Brooks, 2009).

Since MRI is non-invasive and more widely available than nuclear neuroimaging, numerous MRI studies have also been used to investigate brain modifications in Parkinson's disease *in vivo*. The most common MRI approach is voxel-based morphometry, which can be used to evaluate cortical atrophy in both cortical and subcortical structures. Several studies have measured grey matter density alterations in Parkinson's disease using this method (Burton *et al*., 2004; Nagano-Saito *et al*., 2005; Summerfield *et al*., 2005; Feldmann *et al*., 2008; Benninger *et al*., 2009; Ibarretxe-Bilbao *et al*., 2009; Wattendorf *et al*., 2009). These studies have revealed, for example, the greater temporal lobe atrophy of demented compared with non-demented patients with Parkinson's disease (Ramirez-Ruiz *et al*., 2005; Summerfield *et al*., 2005; Ibarretxe-Bilbao *et al*., 2008). However, voxel-based morphometry investigations have not obtained consistent results regarding the differences between non-demented patients with Parkinson's disease and healthy subjects. One voxel-based morphometry study found no difference between these groups (Price *et al*., 2004), while others found atrophy in different anatomical regions, such as the frontal cortex (Burton *et al*., 2004; Nagano-Saito *et al*., 2005), caudate nucleus (Brenneis *et al*., 2003), hippocampus or superior temporal gyrus (Summerfield *et al*., 2005). Furthermore, no differences between non-demented patients with Parkinson's disease and healthy subjects were seen when changes in the grey matter were measured by volumetry from regions of interest (Schulz *et al*., 1999; Cordato *et al*., 2002; Ghaemi *et al*., 2002).

Parkinson-induced prefrontal cortical changes are essentially functional and result from dopaminergic deafferentation in the basal ganglia (Alexander *et al*., 1986). This may explain why there has been a lack of reliable results from magnetic resonance (MR) cortical atrophy studies in non-demented patients with Parkinson's disease. Functional neuroimaging studies of patients with Parkinson's disease performing a simple motor task clearly demonstrate reduced activation (reflected in reduced regional cerebral blood flow) at the level of the main cortical regions that receive afferents from the basal ganglia, including the supplementary motor area (Rascol *et al*., 1992; Sabatini *et al*., 2000), dorsolateral prefrontal cortex (Playford *et al*., 1992) and anterior cingulate gyrus (Jahanshahi *et al*., 1995). Taken together, these results indicate that cortical-level structural MRIs such as voxel-based morphometry have not provided substantial contributions to Parkinson's disease diagnosis.

Other MRI techniques have demonstrated more consistent and promising results from exploring microstructural modifications at the basal ganglia and mesencephalic levels. One such way to explore brain modifications via MR is through diffusion tensor imaging (DTI). This method provides quantitative parameters (Le Bihan, 1995), such as the mean diffusivity that increases with microscopic barrier disruption and extracellular fluid accumulation, and the fractional anisotropy that provides information on the microstructural integrity of highly oriented microstructures (e.g. myelin) (Abe *et al*., 2002). Both mean diffusivity and fractional anisotropy are highly influenced by physiological ageing (Cherubini *et al*., 2009*b*). Furthermore, previous DTI studies on patients with Parkinson's disease have demonstrated a decrease in fractional anisotropy in the substantia nigra compared with healthy controls (Yoshikawa *et al*., 2004; Chan *et al*., 2007; Vaillancourt *et al*., 2009).

Another potential MRI technique is the quantification of mineral levels in the brain. In the last decade, efforts have been made to find a sensitive, reliable method such as MR relaxometry to evaluate the brain iron content *in vivo* (Ordidge *et al*., 1994; Gorell *et al*., 1995; Bartzokis *et al*., 1997; Gelman *et al*., 1999; Graham *et al*., 2000; Jensen *et al*., 2006; Péran *et al*., 2007). Iron metabolism dysregulation and iron accumulation in various parts of the brain are implicated in the pathogenesis of many neurodegenerative diseases, including Parkinson's disease (for a review, see Moos and Morgan, 2004; Zecca *et al*., 2004). Moreover, increased iron content is consistently reported post-mortem in the substantia nigra of patients with Parkinson's disease (Dexter *et al*., 1987; Griffiths and Crossman, 1993; Griffiths *et al*., 1999). This latter observation has been confirmed *in vivo* by transcranial sonography (Berg, 2009) and various MRI techniques (Ordidge *et al*., 1994; Martin *et al*., 2008). The study of microstructural modifications of the substantia nigra appears to be crucial to investigating the physiopathological mechanisms of Parkinson's disease. Indeed, the major pathologic degeneration of Parkinson's disease is the loss of dopaminergic neurons in the substantia nigra pars compacta.

An approach measuring MR parameters sensitive to complementary tissue characteristics (e.g. volume atrophy, iron deposition and microstructural damage) in Parkinson's disease brains could have great potential for investigating pathological changes. Recently, multimodal MRI was used to characterize the

physiological ageing of deep grey matter nuclei in healthy subjects (Cherubini *et al*., 2009*a*). This previous study revealed that physiological ageing does not influence the same parameters in the functioning anatomical region. Overall, the best predictors of physiological ageing were iron deposition in the putamen, and microstructural damage and atrophy in the thalamus. Multimodal MRI may therefore be a valid tool to measure the microstructural integrity of brain structures.

The present work was designed to overcome the limitations of previous single MR parameter studies. We simultaneously measured volume, DTI scalars and T_2* relaxation rates in six deep grey matter structures (thalamus, putamen, caudate, pallidum, substantia nigra and red nucleus) in patients with Parkinson's disease and healthy controls. The aims of the study were (i) to assess changes occurring in idiopathic patients with Parkinson's disease compared with controls, as well as the relationship of these changes to clinical data, and (ii) to discriminate patients with Parkinson's disease from healthy individuals using multimodal MRI.

Materials and methods

Subjects

All participants provided written informed consent. This study was approved by the Santa Lucia Foundation ethics committee. Thirty right-handed patients with Parkinson's disease were included. Parkinson's disease was diagnosed by a staff neurologist, on the basis of akinesia associated with tremor and/or rigidity and responsiveness to levodopa therapy. All patients with Parkinson's disease fulfilled the UK Parkinson's Disease Brain Bank criteria for the diagnosis of idiopathic Parkinson's disease. No patient had a history of neurological or psychiatric disease other than Parkinson's disease. All patients were on anti-parkinsonian medication at the time of testing. The levodopa equivalent daily dose (LEDD) was calculated for each patient (Brodsky *et al*., 2003). Patient motor disabilities were evaluated using the motor part of the Unified Parkinson's Disease Rating Scale (UPDRS). Patients who had end-of-dose motor fluctuations were always tested in the ON phase. Patients who scored <25 on the Mini Mental State Examination were excluded to avoid inclusion of demented patients with Parkinson's disease. A control group of 22 right-handed subjects closely matched to the patients with Parkinson's disease for age, sex and education was also included. None of these control individuals had a history of head injury, stroke or any neurological or psychiatric diseases. Subjects were recruited from community recreational centres, hospital personnel and patients' relatives. Two expert radiologists examined all MRIs to exclude potential brain abnormalities and subjects with microvascular lesions, as apparent from conventional fluid-attenuated inversion recovery (FLAIR) and T_2-weighted images. All subjects (patients and controls) displayed normal conventional imaging results. The demographic and clinical data of the two groups are reported in Table 1.

Acquisition

Participants were examined using a 3 T Allegra MR Imager (Siemens Medical Solutions, Erlangen, Germany) with a standard quadrature head coil. All participants underwent the same MRI protocol, including whole-brain T_2*-weighted, T_1-weighted, DTI, conventional T_2-weighted and FLAIR scanning. All planar sequence acquisitions were acquired along the anterior/posterior commissure line. Particular care was taken to centre the subject in the head coil and to restrain subject movements with cushions and adhesive medical tape.

Six consecutive T_2*-weighted gradient-echo whole-brain volumes were acquired using a segmented echo-planar imaging sequence at different echo times: 6, 12, 20, 30, 45 and 60 ms (repetition time = 5000; bandwidth = 1116 Hz/voxel; matrix size 128×128; 80 axial slices; flip angle 90°; voxel size of $1.8 \times 1.8 \times 1.8\,mm^3$). Diffusion-weighted volumes were acquired using spin-echo echo-planar imaging (echo time/repetition time = 89/8500 ms, bandwidth = 2126 Hz/voxel; matrix size 128×128; 80 axial slices, voxel size $1.8 \times 1.8 \times 1.8\,mm^3$) with 30 isotropically distributed orientations for the diffusion-sensitizing gradients at a *b*-value of 1000 s mm^2 and six $b = 0$ images. Scanning was repeated three times to increase the signal-to-noise ratio. Since the DTI and T_2* volumes each consisted of $128 \times 128 \times 80$ identical isotropic voxels, the slice positioning and orientation of the diffusion-weighted volumes were set to be identical with the T_2* volumes to improve subsequent coregistration. Finally, whole-brain T_1-weighted images were obtained in the sagittal plane using a modified driven equilibrium Fourier transform sequence (Deichmann *et al.*, 2004) (echo time/repetition time = 2.4/7.92 ms, flip angle 15°, voxel size $1 \times 1 \times 1\,mm^3$). The total duration of the imaging protocol was 45 min.

Post-processing

Image processing was performed using FSL 4.1 (FMRIB Software Library; www.fmrib.ox.ac.uk/fsl/) and an in-house software developed in Matlab (version 6.5, The MathWorks), with procedures similar to those described earlier (Cherubini *et al*., 2009*a*; Péran *et al*., 2009). Anatomical regions of interest on the T_1-weighted images were obtained automatically with the segmentation tool FMRIB Integrated Registration and Segmentation Tool (FIRST) 1.2 integrated within

Table 1 Demographic and clinical data of patients with Parkinson's disease and controls

	Sex (M/F)	Age (years)	Disease duration (years)	Hoen and Yahr stage (I/II)	UPDRSm	UPDRSm (MAS)[a]	UPDRSm (LAS)[a]	LEDD[b]
PD	20/10	61.9 ± 11.1	4.5 ± 2.5	10/20	12.0 ± 5.9	6.5 ± 3.2	2.2 ± 2.6	886.8 ± 399.5
Controls	11/11	57.4 ± 9.7	–	–	–	–	–	–

[a]Limb evaluation more affected side (MAS) / limb evaluation less affected side (LAS).
UPDRSm = motor part of UPDRS; PD = Parkinson's disease. [b]LEDD= [levodopa (× 1.2 if catechol-O-methyltransferase (COMT) inhibitor) (× 1.2 if 10 mg of selegiline or × 1.1 if 5 mg of selegiline)] + [pramipexole × 400] + [Ropinirole × 40] + [Cabergoline × 160] + [pergolide × 200] + [bromocriptine × 10] + [lisuride × 160]; all doses are in mg.

the FSL software. In each subject, four deep grey matter structures (thalamus, putamen, caudate and pallidum) were segmented. The substantia nigra and red nucleus were manually segmented using mean T_2*-weighted images by two trained radiologists who were blinded to group membership and clinical information. The images were magnified ×4 before tracing. The substantia nigra is located in the mesencephalon, posterior (dorsal) to the crus cerebri, anterior (ventral) to the midbrain tegmentum and laterally to the red nucleus. The high T_2* contrast-to-noise ratio of our images allowed us to discriminate the mesencephalic structures from the surrounding white matter (Péran *et al*., 2007). Based on previous MR studies (Massey *et al*., 2010), the substantia nigra was identified as the band of signal hypointensity on T_2* in the midbrain on each slice (4–6 continuous slices). The red nucleus was also identified using signal hypointensity on a different slice (3–4 continuous slices). For each subject, voxels that were considered to be of the substantia nigra or red nucleus were those included by both radiologists. A DTI model was fit at each voxel, generating fractional anisotropy and mean diffusivity maps. The fractional anisotropy maps were then registered to brain-extracted whole-brain volumes from T_1-weighted images using a full affine (correlation ratio cost function) alignment with nearest-neighbour resampling. The calculated transformation matrix was then applied to the mean diffusivity maps with identical resampling options.

The six T_2*-weighted volumes were averaged to generate a mean T_2*-weighted volume. A full affine 3D alignment was calculated between each of the six T_2*-weighted volumes and the mean T_2*-weighted volume. For each subject, a voxel-by-voxel nonlinear least-squares fitting of the data was acquired at the six echo times to obtain a mono-exponential signal decay curve ($S = S_0 e^{-t/T_2^*}$). This method, combining data acquisition and data processing of T_2* images, demonstrated good reproducibility (Péran *et al.,* 2007). To facilitate analysis of the relaxation results, we considered the inverse of the relaxation times (i.e. relaxation rates $R_2^* = 1/T_2^*$) as described earlier (Cherubini *et al.,* 2009a, *b*; Péran *et al.,* 2007, 2009). The mean T_2*-weighted volume was registered to the T_1-weighted volume using a full affine alignment. The calculated transformation matrix was then applied to the R_2* maps with nearest-neighbour resampling options, as well as to the manually segmented regions (substantia nigra and red nucleus). As a result of this processing, the mean diffusivity, fractional anisotropy and R_2* maps were corrected for head movements, and shared an identical reference space with the anatomical T_1-weighted volumes.

For each subject and each hemisphere, the volumes of the segmented subcortical areas were calculated. To reduce the effects of inter-individual variability in head size, individual volume values were multiplied by a normalization factor obtained with the SIENAX tool (http://www.fmrib.ox.ac.uk/fsl/siena/index.html) from the corresponding T_1-weighted image. This normalization factor was derived from the normalizing transform; the brain image was affine-registered to a template, and a multiplying factor was calculated from the transformation matrix itself, using the skull image to determine the registration scaling.

For each subject, the region of interest segmentation results, coregistered fractional anisotropy map and coregistered R_2* map were all superimposed onto the original T_1-weighted volume. The resulting images were visually assessed by two trained radiologists to exclude misregistration or erroneous region of interest identification. The segmented structures defined the binary masks, where the mean values of mean diffusivity, fractional anisotropy and R_2* were calculated for each individual. The T_1-weighted volume was registered to the Montreal Neurological Institute template using FMRIB's (Functional Magnetic Resonance Imaging of the Brain, University of Oxford) non-linear image registration tool (http://www.fmrib.ox.ac.uk/fsl/fnirt/index.html). This spatial transformation was applied to each subject to coregister R_2*, mean diffusivity and fractional anisotropy maps on the Montreal Neurological Institute template. To determine the probability of a particular voxel in Montreal Neurological Institute space being occupied by a structure of interest, the frequency at which the structure of interest resided at a particular voxel was assessed across the 52 data sets. Unit increments in voxel intensity correspond to an increase in the probability of encountering a particular structure at that location in 1/52 = 1.9% of data sets (see Supplementary Material).

Statistical analysis

For each of the six deep grey matter structures, the volume, R_2*, mean diffusivity and fractional anisotropy were used to perform statistical region- and voxel-based analyses.

Region-based analysis

The mean values of R_2*, fractional anisotropy, mean diffusivity and volume were compared using a repeated-measures multivariate analysis of covariance (MANCOVA) with three factors (group, anatomical region, lateralization) and with age as covariate. Then, a two-way MANCOVA with group and lateralization as factors and age as covariate was applied to each parameter and each structure. For each significant result, multiple regression analysis for the given anatomical region was conducted between clinical data (age, disease duration, LEDD, motor part of UPDRS) and the respective MR parameter.

Voxel-based analysis

The R_2*, mean diffusivity and fractional anisotropy values were compared using a two-sample unpaired *t*-test with age as covariate. Significant subregions were those with values above a threshold of $P < 0.01$, based on threshold-free cluster enhancement (minimum cluster size = 50). For each subregion associated with a specific MR parameter (R_2*, mean diffusivity or fractional anisotropy), the mean values were extracted for all participants. Multiple regression analysis was conducted between clinical data (age, disease duration, LEDD and motor part of UPDRS) and the respective MR parameter/subregion pair mean.

Predictive analysis and ROC curves

Since one of the main goals of the study was to discriminate patients with Parkinson's disease from controls, logistic regressions and receiver operating characteristic (ROC) curves were computed using the mean of each MR parameter/subregion pair individualized from the previous voxel-based analysis. All combinations among these pairs were tested to determine the combinations with the best discriminating power. A repeated 10-fold cross-validation was performed to calculate the area under the ROC curve for each combination. Combinations with areas under the curve of >95% are reported.

Results

The probabilistic map (see Supplementary Material) indicated that the identification of anatomical regions (using automatic and manual segmentation) and spatial registration were accurately assessed, according to the results of Péran *et al*. (2009).

Differences between patients with Parkinson's disease and controls

Patients with Parkinson's disease displayed significantly higher R_2* values in the substantia nigra, lower fractional anisotropy values in the substantia nigra and thalamus, and higher mean diffusivity values in the thalamus than control subjects (Table 2 and Fig. 1). Voxel-based analyses confirmed the previous localizations and identified differences for the mean diffusivity in the striatum (Table 3 and Fig. 2).

Multiple regressions with clinical data

The anatomical region and subregion analyses revealed strong correlations between age and mean diffusivity values, and between age and fractional anisotropy values in the thalamus (Table 4). A positive relationship was also observed between R_2* values and LEDD scores in the right substantia nigra, when the entire substantia nigra or subregions of the substantia nigra were considered.

Predictive analysis

Logistic regression analysis showed that combinations of three different markers were sufficient to obtain >95% discrimination between patients with Parkinson's disease and controls (maximum area under the curve: 98%, Fig. 3A). The markers comprising the discriminating combinations were: (R_2* values in left or right substantia nigra) + (fractional anisotropy values in right substantia nigra) + (mean diffusivity in putamen or caudate nucleus) (Fig. 3B). Logistic regressions were also computed for combinations of four markers. The discriminating power of the four-marker combinations did not increase significantly (maximum area under the curve: 99%), and the distribution of markers, characterized by their percentage of presence in the discriminant combinations, confirmed the previous findings, since the markers comprising the three-marker combinations were the ones with a higher percentage of presence: fractional anisotropy/right substantia nigra: 98%, mean diffusivity/right putamen: 52%, R_2*/left substantia nigra: 52%, R_2*/right substantia nigra: 40%, mean diffusivity/right caudate nucleus$_1$: 38%, fractional anisotropy/left putamen: 24%, mean diffusivity/right caudate nucleus$_2$: 22%, mean diffusivity/left thalamus$_2$: 16%, mean diffusivity/left substantia nigra: 14%, fractional anisotropy/right thalamus: 12%, mean diffusivity/right thalamus$_2$: 12%, mean diffusivity/left thalamus$_1$: 10% and mean diffusivity/right thalamus$_1$: 10%. Furthermore, it is important to note that the discriminant power in considering only one marker at a time comprises 71–83% (for the main markers: fractional anisotropy/right substantia nigra: 77%, mean diffusivity/right putamen: 83%, R_2*/left substantia nigra: 77%, R_2*/right substantia nigra: 75% and mean diffusivity/right caudate nucleus$_1$: 75%).

Discussion

We used multimodal MRI to quantify subcortical changes in patients with idiopathic Parkinson's disease. Our work on a large group of non-demented patients with Parkinson's disease showed mainly an increase in R_2* values and a decrease in fractional anisotropy values in the substantia nigra, and a decrease in the mean diffusivity values in the striatum compared with healthy subjects. Taken together, our findings reveal that multimodal MRI is able to discriminate patients with Parkinson's disease from healthy control subjects.

Predictive markers

The results of the ROC and cross-validated discrimination analyses demonstrated that combinations of three different markers were sufficient to obtain >95% discrimination between patients with Parkinson's disease and healthy controls. The markers comprising the discriminating combinations were the R_2* and fractional

Table 2 MANCOVAs from region-based analysis: volume, R_2*, mean diffusivity and fractional anisotropy

	Volume	R_2*	Mean diffusivity	Fractional anisotropy
Global MANCOVA				
Main effect group	ns	ns	ns	ns
Interaction Group × Anatomical Region	ns	$F = 1.94$; $P = 0.09$	ns	$F = 2.29$; $P < 0.05$
MANCOVA for anatomical region				
Thalamus				
Main effect group	ns	ns	$F = 11.33$; $P < 0.05$	$F = 5.07$; $P < 0.05$
Putamen				
Main effect group	ns	ns	ns	ns
Caudate nucleus				
Main effect group	ns	ns	ns	ns
Pallidum				
Main effect group	ns	ns	ns	ns
Substantia nigra				
Main effect group	ns	$F = 5.9$; $P < 0.02$	ns	$F = 4.94$; $P < 0.05$
Red nucleus				
Main effect group	ns	ns	ns	ns

ns: non significant.

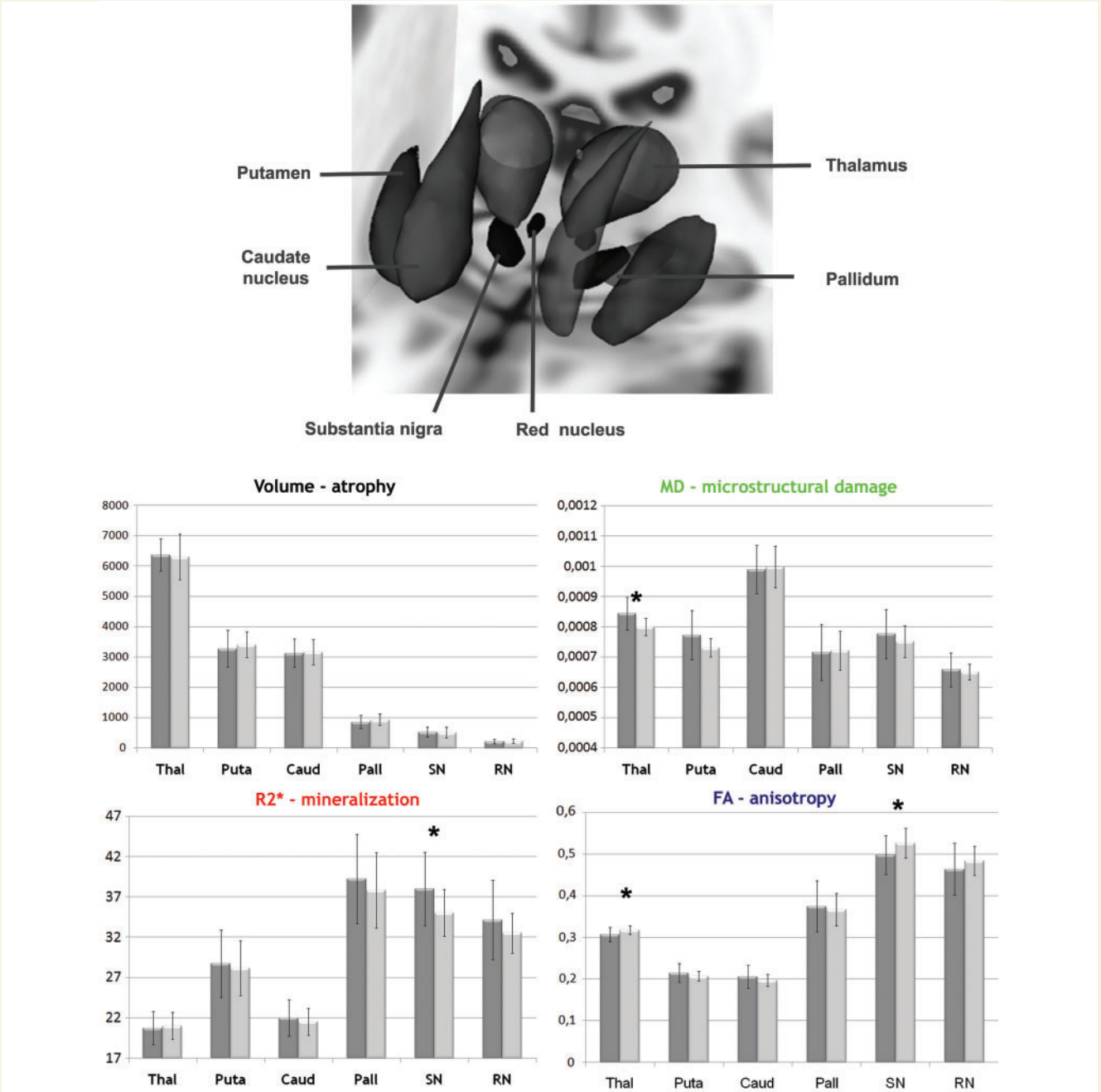

Figure 1 3D reconstruction of subcortical regions considered in this work (top). Volume (mm^3), R_2* (s^{-1}), mean diffusivity (mm^2s^{-1}) and fractional anisotropy mean values from whole subcortical structures (bottom). Light bars = controls, darker bars = Parkinson's disease. *Significant difference.

anisotropy in the substantia nigra, and the mean diffusivity in the putamen or caudate nucleus (Fig. 3). Unsurprisingly, the predictive markers involved the nigrostriatal structures that characterize Parkinson's disease physiopathology. The highly discriminating combinations were composed of markers from three different MR parameters (R_2*, mean diffusivity and fractional anisotropy), suggesting that the MR parameters provide different but complementary information. Indeed, taken individually, none of the markers reached as high a discriminant power as those obtained in combination.

Two recent studies have shown MRI-guided discrimination between patients with Parkinson's disease and controls. The first study revealed that fractional anisotropy in the substantia nigra distinguishes early-stage patients with Parkinson's disease from healthy individuals (Vaillancourt *et al*., 2009). In this previous work, regions of interest were manually drawn using small circles in the substantia nigra localized from a single DTI slice and did not consider the nigral subdivisions (pars reticularis or pars compacta). In our study, the regions of interest correspond to the entire substantia nigra. The second study (Menke *et al*., 2009), using

Table 3 Voxel-based analysis

Clusters	Voxels	*P*-value	Mean (±SD)	
			Patients with Parkinson's disease	Controls
R_2*/right substantia nigra and red nucleus	207	<0.001	33.34 (±4.72)	29.89 (±2.08)
R_2*/left substantia nigra and red nucleus	215	<0.001	32.27 (±3.90)	29.02 (±2.11)
Mean diffusivity/right thalamus 1	1242	<0.001	864.65 (±64.42)	802.68 (±28.36)
Mean diffusivity/right putamen	854	<0.0001	773.72 (±79.66)	703.60 (±36.74)
Mean diffusivity/left thalamus 1	287	<0.001	771.22 (±39.42)	735.95 (±19.88)
Mean diffusivity/right caudate nucleus 1	213	<0.001	806.85 (±94.58)	726.86 (±39.24)
Mean diffusivity/ right caudate nucleus 2	105	<0.005	795.52 (±82.34)	733.79 (±51.83)
Mean diffusivity/ right thalamus 2	83	<0.001	1377.03 (±249.80)	1162.92 (±185.49)
Mean diffusivity/ left thalamus 2	72	<0.005	746.09 (±50.50)	709.76 (±18.75)
Mean diffusivity/ left substantia nigra	53	<0.0001	844.53 (±53.12)	776.20 (±44.90)
Fractional anisotropy/right thalamus	803	<0.001	0.25 (±0.03)	0.29 (±0.020)
Fractional anisotropy/right substantia nigra	109	<0.001	0.42 (±0.03)	0.46 (±0.030)
Fractional anisotropy/left putamen	312	<0.001	0.21 (±0.03)	0.18 (±0.018)

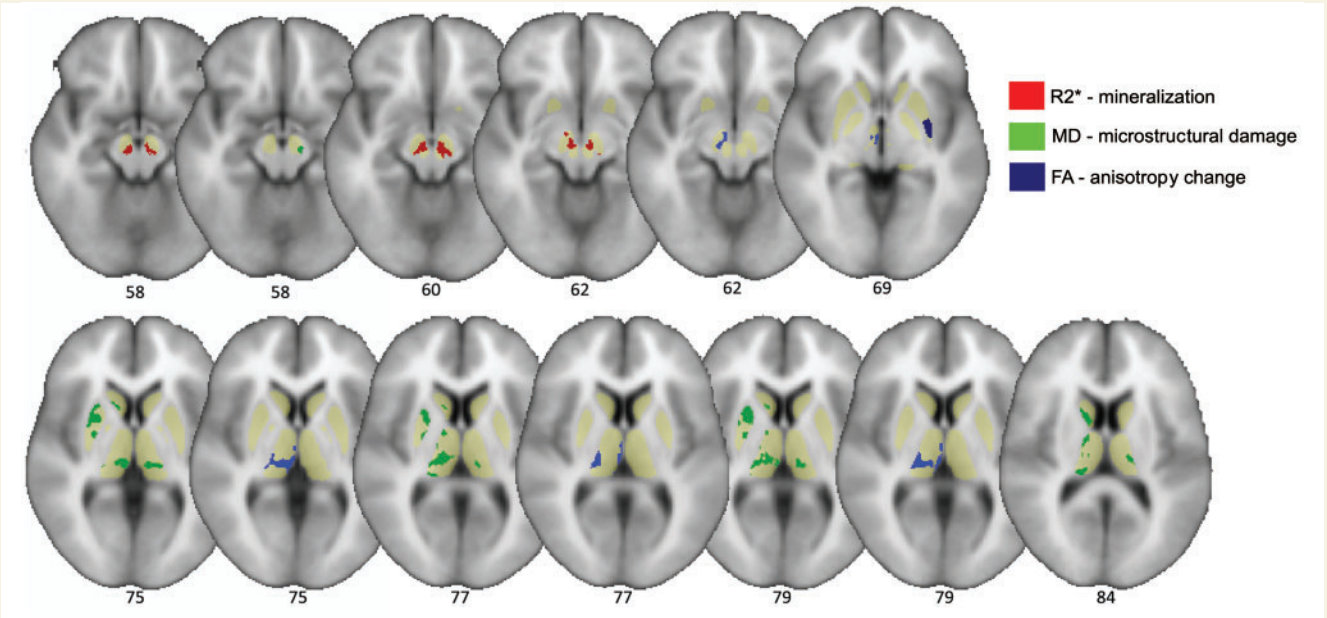

Figure 2 Differences between patients with Parkinson's disease and controls from voxel-based analysis of R_2*, mean diffusivity and fractional anisotropy maps. The *z*-position on the template is indicated under each slice. The light yellow corresponds to the investigated regions.

driven equilibrium single pulse observation of T_1 to identify the substantia nigra, combined volumetry of the substantia nigra and its connectivity with the thalamus to achieve a good sensitivity (100%) and specificity (80%) for classifying patients with Parkinson's disease. It is important to note that our MR study assessed ROC analysis with a larger number of patients with Parkinson's disease than in these previous works. Despite the difference of DTI data acquisition and DTI data analysis with Vaillancourt's study (2009), the results of the present study not only confirm the importance of fractional anisotropy in the substantia nigra to discriminate patients with Parkinson's disease from healthy subjects but also demonstrate the utility of considering multiple parameters.

Iron content also played a key role in the substantia nigra and microstructural damage in the striatum of patients with Parkinson's disease. Using the same methodology as ours, a recent study revealed that the best predictor of physiological ageing is iron deposition in the striatum (Cherubini *et al*., 2009*a*).

Our findings also confirm the crucial role of the substantia nigra in Parkinson's disease. Previous MR studies confined substantia nigra quantification to area measurements within a few selected slices through the midbrain, rather than the whole substantia nigra volume (Martin *et al*., 2008; Vaillancourt *et al*., 2009). In contrast, we considered all mesencephalic structures (red nucleus and substantia nigra) identified on high-resolution T_2*-weighted images (Péran *et al*., 2007). Since substantia nigra degeneration is not

Table 4 Multiple regression analysis with clinical data

	Age p(β)	Disease duration p(β)	LEDD p(β)	Left side UPDRSm p(β)	Right side UPDRSm p(β)
Modality/ anatomical region					
R_2*-SN					
Right	0.92 (−0.02)	0.2 (−0.25)	**<0.05 (0.93)**	0.83 (−0.04)	0.09 (0.33)
Left	0.85 (0.04)	0.43 (−0.17)	0.27 (0.23)	0.78 (−0.07)	0.12 (0.33)
MD-Thal					
Right	**<0.00 (0.78)**	0.20 (−0.18)	0.25 (0.16)	0.64 (0.08)	0.77 (0.04)
Left	**<0.00 (0.78)**	0.79 (−0.04)	1.00 (0.00)	0.75 (0.05)	0.99 (0.00)
FA-SN					
Right	0.94 (0.02)	0.98 (−0.01)	0.18 (−0.28)	0.25 (0.28)	0.55 (−0.12)
Left	0.22 (−0.30)	0.87 (0.04)	0.65 (−0.10)	0.46 (−0.18)	0.54 (0.13)
FA-Thal					
Right	**<0.01 (−0.59)**	0.75 (−0.06)	0.21 (−0.23)	0.17 (−0.29)	0.37 (0.16)
Left	**<0.00 (−0.63)**	0.54 (−0.11)	0.31 (−0.18)	0.24 (−0.24)	0.12 (0.28)
Modality/subregion					
R_2*/right SN	0.11 (−0.35)	0.73 (−0.06)	**<0.03 (0.42)**	0.27 (−0.24)	0.35 (0.17)
R_2*/left SN	0.20 (−0.31)	0.67 (−0.09)	0.34 (0.20)	0.37 (−0.22)	0.32 (0.21)
MD/right putamen	**<0.01 (0.55)**	0.95 (0.01)	0.29 (0.19)	0.68 (0.08)	0.10 (−0.30)
MD/right thalamus 1	**<0.00 (0.84)**	0.74 (−0.05)	0.35 (−0.13)	0.35 (0.15)	0.69 (0.05)
MD/left thalamus 1	**<0.00 (0.88)**	0.13 (−0.20)	0.82 (−0.03)	0.14 (0.22)	0.67 (0.05)
MD/left thalamus 2	**<0.00 (0.85)**	0.76 (0.04)	0.13 (−0.22)	0.13 (0.25)	0.12 (−0.22)
MD/right thalamus 2	**<0.00 (0.80)**	0.49 (−0.10)	0.58 (−0.08)	0.45 (0.13)	0.31 (0.15)
MD/left SN	**<0.01 (0.49)**	0.74 (0.06)	0.30 (−0.17)	0.25 (−0.22)	0.26 (0.19)
MD/right CN1	**<0.00 (0.71)**	0.55 (−0.10)	0.15 (−0.24)	0.34 (0.18)	0.86 (−0.03)
MD/right CN2	**<0.05 (0.47)**	0.58 (−0.11)	0.61 (0.10)	0.30 (0.25)	0.67 (−0.09)
FA/right thalamus	**<0.00 (−0.74)**	0.33 (−0.17)	0.97 (0.01)	0.16 (−0.27)	0.86 (−0.03)
FA/right SN	0.91 (−0.03)	0.28 (−0.24)	0.58 (−0.12)	0.84 (−0.05)	0.82 (0.05)
FA/left putamen	0.76 (−0.07)	0.69 (0.09)	0.99 (0.00)	0.81 (0.06)	0.44 (0.17)

MD = mean diffusivity; SN = substantia nigra; Thal = thalamus; FA = fractional anisotropy; CN = caudate nucleus. Significant values are indicated in bold.

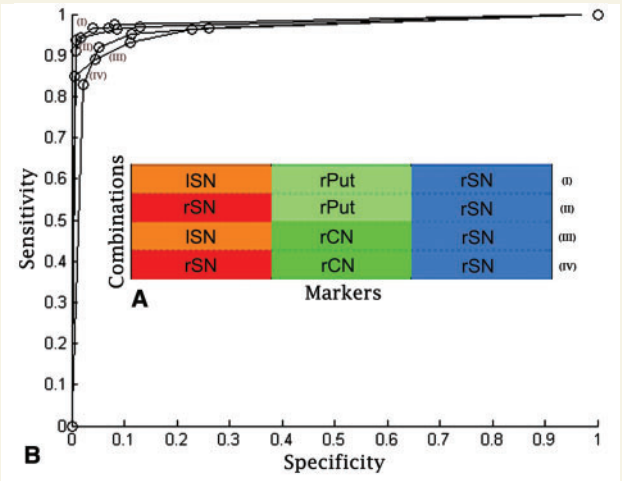

Figure 3 In the centre box (**A**) we show the combinations of MR parameters that were able to significantly discriminate between patients with Parkinson's disease and controls. Colours indicate the parameters (red = R_2*, green = mean diffusivity, blue = fractional anisotropy) while acronyms identify the anatomical regions of interest indicated. Combinations are numbered from I to IV based on discriminant power (95–98%). (**B**) ROC curves associated with each significant combination.

homogeneous (Fearnley and Lees, 1991), a voxel-level analysis was used to address the subregions that are more susceptible to Parkinson's disease-associated changes. In contrast to previous studies where the localization of substantia nigra subregions was manually defined prior to statistical analysis (Martin *et al*., 1998; Vaillancourt *et al*., 2009), here this region was the product of the voxel-based analysis from the R_2* and fractional anisotropy values. The subregion that emerged from our voxel-based analysis is located in the posterior-medial portion of substantia nigra, which could correspond to the anatomical localization to the substantia nigra pars compacta, particularly sensitive to Parkinson's disease. The exact and complete segmentation of the substantia nigra and red nucleus on MRI must be considered with caution (for a review, see Massey *et al*., 2010). However, high-resolution images combined with voxel-based analysis in the present work as well as in a recent study (Baudrexel *et al*., 2010) are a promising way to study microstructural modifications in mesencephalic structures.

The gold standard of Parkinson's disease diagnosis is neuropathology, and misdiagnosis in some clinically diagnosed patients cannot be excluded (Hughes *et al*., 1992; Jankovic *et al*., 2000; Tolosa *et al*., 2006). Here, we tested a group of non-demented medicated patients with moderate Parkinson's disease. Most diagnostic errors occur in early disease stages (Osaki *et al*., 2002;

Tolosa *et al*., 2006), and the disease duration, history and dopaminergic treatment efficacy tend to consolidate Parkinson's disease diagnosis. Despite presenting with clinical markers of Parkinson's disease, the conventional MR examinations of our patients were classified as normal by both radiologists. However, we achieved good individual discrimination in the Parkinson's disease patient group, which presented with a discrete spectrum of drug treatments, disease durations and motor disabilities. As a consequence, the observed nigrostriatal signature of the Parkinson's disease population can be considered as relatively generic and not specific to one category of patients with Parkinson's disease. Considering the results of the present study, the multimodal MRI approach provides evidence that physiological and pathological processes can be described by different MR parameters that provide different but complementary measures of microstructural modifications.

Magnetic resonance biomarkers and Parkinson's disease physiopathology

We utilized relaxation rates such as R_2* as an indirect measure of the iron level in the deep grey matter. Our region-based results showed an increase in R_2* only in the substantia nigra. The subregion of the substantia nigra that could correspond to the pars compacta is also more sensitive to increases in R_2* (Fig. 2). Iron-level increases in the substantia nigra pars compacta of post-mortem Parkinson's disease patient brains were first reported in 1924 (Lehermitte and McAlpine, 1924). Since then, numerous histochemical studies (Dexter *et al*., 1987; Sofic *et al*., 1991) and MR studies (Graham *et al*., 2000; Martin *et al*., 2008; Baudrexel *et al*., 2010) have confirmed this specific iron accumulation. The increased substantia nigra iron content is generally thought to represent dopaminergic neuronal loss. This interpretation is consistent with the significant relationship found between the R_2* and LEDD in the substantia nigra, both throughout the whole structure and the subregion of the substantia nigra. This result must be considered with caution, since the correlation was found with only the right substantia nigra. Although further investigations are required, the link between dopaminergic drug treatment and dopaminergic loss in the substantia nigra appears promising.

Previous studies using DTI showed that fractional anisotropy in the substantia nigra is reduced in patients with Parkinson's disease compared with healthy subjects (Yoshikawa *et al*., 2004; Chan *et al*., 2007; Vaillancourt *et al*., 2009). Likewise, we also observed lower mean fractional anisotropy values in the substantia nigra of patients with Parkinson's disease compared with control subjects. Histochemical analyses of a Parkinson's disease animal model showed that DTI can be used to assess nigrostriatal degeneration by measuring the decrease of fractional anisotropy in the substantia nigra (Boska *et al*., 2007).

Our results also revealed an increase in the mean diffusivity in the striatum subregions of patients with Parkinson's disease. One possible interpretation for this alteration is the deafferentation of the nigrostriatal pathway, since striatal dopaminergic denervation induces a complex microstructural reorganization. While the observed non-correlation between striatum mean diffusivity and motor scale does not corroborate this interpretation, it should be noted that our patients were on dopaminergic medication, which masks the real state of movement disorders. Since such findings have never been reported before, further studies are required to corroborate our interpretation.

Apart from markers included in the discriminant signature, we also found other markers for which differences were found between patients with Parkinson's disease and controls. For example, we found lower mean diffusivity values in patients with Parkinson's disease in the thalamus from anatomical region analysis than from voxel-based analysis. However, the mean diffusivity in the thalamus also exhibited a strong relationship with age in our Parkinson's disease population. In consequence, new investigations will be necessary to understand whether these markers play a specific role in Parkinson's disease physiopathology.

Our study investigated patients with moderate Parkinson's disease on medication. Longitudinal studies on large cohorts of patients with Parkinson's disease will be crucial to confirm our results and to follow accurately the brain modifications due to Parkinson's disease progression. Further studies will also be necessary to define potential specific signatures of different Parkinson's disease subgroups (e.g. *de novo* patients, patients with predominant akinesia versus predominant tremor, patients with frozen gait) or differences between Parkinson's disease and atypical parkinsonian syndromes such as multiple system atrophy and progressive supranuclear palsy. Another crucial investigation will be to study the effects of anti-parkinsonian medication to assess whether MR measures changes in the OFF state compared with the ON state, as well as the relationship of these changes to clinical data.

Conclusion

This study demonstrates that multimodal MRI is able to identify the nigrostriatal signature of Parkinson's disease using specific MRI markers and to discriminate patients with Parkinson's disease from healthy control subjects with a high accuracy. The combination of different MR biomarkers opens new perspectives to investigate pathological changes, such as disease progression and long-term drug impact, detecting non-dopaminergic degeneration and evaluating neuroprotective effects.

Funding

INSERM-DHOS 2007-2009 grant and Italian Ministry of Health grant (RF07.97.5).

Supplementary material

Supplementary material is available at *Brain* online.

References

Abe O, Aoki S, Hayashi N, Yamada H, Kunimatsu A, Mori H, et al. Normal aging in the central nervous system: quantitative MR diffusion-tensor analysis. Neurobiol Aging 2002; 23: 433–41.

Alexander GE, DeLong MR, Strick PL. Parallel organization of functionally segregated circuits linking basal ganglia and cortex. Annu Rev Neurosci 1986; 9: 357–81.

Bartzokis G, Beckson M, Hance DB, Marx P, Foster JA, Marder SR. MR evaluation of age-related increase of brain iron in young adult and older normal males. Magn Reson Imaging 1997; 15: 29–35.

Baudrexel S, Nürnberger L, Rüb U, Seifried C, Klein JC, Deller T, et al. Quantitative mapping of T1 and T2* discloses nigral and brainstem pathology in early Parkinson's disease. Neuroimage 2010; 51: 512–20.

Benninger DH, Thees S, Kollias SS, Bassetti CL, Waldvogel D. Morphological differences in Parkinson's disease with and without rest tremor. J Neurol 2009; 256: 256–63.

Berg D. Transcranial ultrasound as a risk marker for Parkinson's disease. Mov Disord 2009; 24 (Suppl 2): S677–83.

Boska MD, Hasan KM, Kibuule D, Banerjee R, McIntyre E, Nelson JA, et al. Quantitative diffusion tensor imaging detects dopaminergic neuronal degeneration in a murine model of Parkinson's disease. Neurobiol Dis 2007; 26: 590–6.

Brenneis C, Seppi K, Schocke MF, Muller J, Luginger E, Bosch S, et al. Voxel-based morphometry detects cortical atrophy in the Parkinson variant of multiple system atrophy. Mov Disord 2003; 18: 1132–8.

Brodsky MA, Godbold J, Roth T, Olanow CW. Sleepiness in Parkinson's disease: a controlled study. Mov Disord 2003; 18: 668–72.

Burton EJ, McKeith IG, Burn DJ, Williams ED, O'Brien JT. Cerebral atrophy in Parkinson's disease with and without dementia: a comparison with Alzheimer's disease, dementia with Lewy bodies and controls. Brain 2004; 127: 791–800.

Caslake R, Moore JN, Gordon JC, Harris CE, Counsell C. Changes in diagnosis with follow-up in an incident cohort of patients with parkinsonism. J Neurol Neurosurg Psychiatry 2008; 79: 1202–7.

Chan LL, Rumpel H, Yap K, Lee E, Loo HV, Ho GL, et al. Case control study of diffusion tensor imaging in Parkinson's disease. J Neurol Neurosurg Psychiatry 2007; 78: 1383–6.

Cherubini A, Péran P, Caltagirone C, Sabatini U, Spalletta G. Aging of subcortical nuclei: microstructural, mineralization and atrophy modifications measured in vivo using MRI. Neuroimage 2009a; 48: 29–36.

Cherubini A, Péran P, Hagberg GE, Varsi AE, Luccichenti G, Caltagirone C, et al. Characterization of white matter fiber bundles with T_2* relaxometry and diffusion tensor imaging. Magn Reson Med 2009b; 61: 1066–72.

Cordato NJ, Pantelis C, Halliday GM, Velakoulis D, Wood SJ, Stuart GW, et al. Frontal atrophy correlates with behavioural changes in progressive supranuclear palsy. Brain 2002; 125: 789–800.

Deichmann R, Schwarzbauer C, Turner R. Optimisation of the 3D MDEFT sequence for anatomical brain imaging: technical implications at 1.5 and 3 T. Neuroimage 2004; 21: 757–67.

Dexter DT, Wells FR, Agid F, Agid Y, Lees AJ, Jenner P, et al. Increased nigral iron content in postmortem parkinsonian brain. Lancet 1987; 2: 1219–20.

Fearnley JM, Lees AJ. Ageing and Parkinson's disease: substantia nigra regional selectivity. Brain 1991; 114 (Pt 5): 2283–301.

Feldmann A, Illes Z, Kosztolanyi P, Illes E, Mike A, Kover F, et al. Morphometric changes of gray matter in Parkinson's disease with depression: a voxel-based morphometry study. Mov Disord 2008; 23: 42–6.

Gelman N, Gorell JM, Barker PB, Savage RM, Spickler EM, Windham JP, et al. MR imaging of human brain at 3.0 T: preliminary report on transverse relaxation rates and relation to estimated iron content. Radiology 1999; 210: 759–67.

Ghaemi M, Hilker R, Rudolf J, Sobesky J, Heiss WD. Differentiating multiple system atrophy from Parkinson's disease: contribution of striatal and midbrain MRI volumetry and multi-tracer PET imaging. J Neurol Neurosurg Psychiatry 2002; 73: 517–23.

Gorell JM, Ordidge RJ, Brown GG, Deniau JC, Buderer NM, Helpern JA. Increased iron-related MRI contrast in the substantia nigra in Parkinson's disease. Neurology 1995; 45: 1138–43.

Graham JM, Paley MN, Grunewald RA, Hoggard N, Griffiths PD. Brain iron deposition in Parkinson's disease imaged using the PRIME magnetic resonance sequence. Brain 2000; 123 (Pt 12): 2423–31.

Griffiths PD, Crossman AR. Distribution of iron in the basal ganglia and neocortex in postmortem tissue in Parkinson's disease and Alzheimer's disease. Dementia 1993; 4: 61–5.

Griffiths PD, Dobson BR, Jones GR, Clarke DT. Iron in the basal ganglia in Parkinson's disease. An in vitro study using extended X-ray absorption fine structure and cryo-electron microscopy. Brain 1999; 122 (Pt 4): 667–73.

Hughes AJ, Daniel SE, Kilford L, Lees AJ. Accuracy of clinical diagnosis of idiopathic Parkinson's disease: a clinico-pathological study of 100 cases. J Neurol Neurosurg Psychiatry 1992; 55: 181–4.

Ibarretxe-Bilbao N, Ramirez-Ruiz B, Junque C, Marti MJ, Valldeoriola F, Bargallo N, et al. Differential progression of brain atrophy in Parkinson disease with and without visual hallucinations. J Neurol Neurosurg Psychiatry 2010; 81: 650–7.

Ibarretxe-Bilbao N, Ramirez-Ruiz B, Tolosa E, Marti MJ, Valldeoriola F, Bargallo N, et al. Hippocampal head atrophy predominance in Parkinson's disease with hallucinations and with dementia. J Neurol 2008; 255: 1324–31.

Jahanshahi M, Jenkins IH, Brown RG, Marsden CD, Passingham RE, Brooks DJ. Self-initiated versus externally triggered movements: I. An investigation using measurement of regional cerebral blood flow with PET and movement-related potentials in normal and Parkinson's disease subjects. Brain 1995; 118 (Pt 4): 913–33.

Jankovic J, Rajput AH, McDermott MP, Perl DP. The evolution of diagnosis in early Parkinson disease. Parkinson Study Group. Arch Neurol 2000; 57: 369–72.

Jensen JH, Chandra R, Ramani A, Lu H, Johnson G, Lee SP, et al. Magnetic field correlation imaging. Magn Reson Med 2006; 55: 1350–61.

Le Bihan D. Molecular diffusion, tissue microdynamics and microstructure. NMR Biomed 1995; 8: 375–86.

Lehermitte JKW, McAlpine MA. On the occurrence of abnormal deposits of iron in the brain in Parkinson's disease with special reference to its location. J Neurol Psychopathol 1924; 5: 195–208.

Martin WR, Wieler M, Gee M. Midbrain iron content in early Parkinson disease: a potential biomarker of disease status. Neurology 2008; 70: 1411–7.

Martin WR, Ye FQ, Allen PS. Increasing striatal iron content associated with normal aging. Mov Disord 1998; 13: 281–6.

Massey LA, Yousry TA. Anatomy of the substantia nigra and subthalamic nucleus on MR imaging. Neuroimaging Clin N Am 2010; 20: 7–27.

Menke RA, Scholz J, Miller KL, Deoni S, Jbabdi S, Matthews PM, et al. MRI characteristics of the substantia nigra in Parkinson's disease: a combined quantitative T1 and DTI study. Neuroimage 2009; 47: 435–41.

Moos T, Morgan EH. The metabolism of neuronal iron and its pathogenic role in neurological disease: review. Ann N Y Acad Sci 2004; 1012: 14–26.

Nagano-Saito A, Washimi Y, Arahata Y, Kachi T, Lerch JP, Evans AC, et al. Cerebral atrophy and its relation to cognitive impairment in Parkinson disease. Neurology 2005; 64: 224–9.

Ordidge RJ, Gorell JM, Deniau JC, Knight RA, Helpern JA. Assessment of relative brain iron concentrations using T2-weighted and T2*-weighted MRI at 3 Tesla. Magn Reson Med 1994; 32: 335–41.

Osaki Y, Wenning GK, Daniel SE, Hughes A, Lees AJ, Mathias CJ, et al. Do published criteria improve clinical diagnostic accuracy in multiple system atrophy? Neurology 2002; 59: 1486–91.

Pavese N, Brooks DJ. Imaging neurodegeneration in Parkinson's disease. Biochim Biophys Acta 2009; 1792: 722–9.

Péran P, Cherubini A, Luccichenti G, Hagberg G, Demonet JF, Rascol O, et al. Volume and iron content in basal ganglia and thalamus. Hum Brain Mapp 2009; 30: 2667–75.

Péran P, Hagberg G, Luccichenti G, Cherubini A, Brainovich V, Celsis P, et al. Voxel-based analysis of *R2** maps in the healthy human brain. J Magn Reson Imaging 2007; 26: 1413–20.

Péran P, Luccichenti G, Cherubini A, Hagberg GE, Sabatini U. High-field neuroimaging in Parkinson's disease. In: Salvolini U, Scarabino T, editors. High field brain MRI. Berlin: Springer; 2006. p. 169–76.

Playford ED, Jenkins IH, Passingham RE, Nutt J, Frackowiak RS, Brooks DJ. Impaired mesial frontal and putamen activation in Parkinson's disease: a positron emission tomography study. Ann Neurol 1992; 32: 151–61.

Price S, Paviour D, Scahill R, Stevens J, Rossor M, Lees A, et al. Voxel-based morphometry detects patterns of atrophy that help differentiate progressive supranuclear palsy and Parkinson's disease. Neuroimage 2004; 23: 663–9.

Ramirez-Ruiz B, Marti MJ, Tolosa E, Bartres-Faz D, Summerfield C, Salgado-Pineda P, et al. Longitudinal evaluation of cerebral morphological changes in Parkinson's disease with and without dementia. J Neurol 2005; 252: 1345–52.

Rascol O, Sabatini U, Chollet F, Celsis P, Montastruc JL, Marc-Vergnes JP, et al. Supplementary and primary sensory motor area activity in Parkinson's disease. Regional cerebral blood flow changes during finger movements and effects of apomorphine. Arch Neurol 1992; 49: 144–8.

Sabatini U, Boulanouar K, Fabre N, Martin F, Carel C, Colonnese C, et al. Cortical motor reorganization in akinetic patients with Parkinson's disease: a functional MRI study. Brain 2000; 123 (Pt 2): 394–403.

Schulz JB, Skalej M, Wedekind D, Luft AR, Abele M, Voigt K, et al. Magnetic resonance imaging-based volumetry differentiates idiopathic Parkinson's syndrome from multiple system atrophy and progressive supranuclear palsy. Ann Neurol 1999; 45: 65–74.

Sofic E, Paulus W, Jellinger K, Riederer P, Youdim MB. Selective increase of iron in substantia nigra zona compacta of parkinsonian brains. J Neurochem 1991; 56: 978–82.

Summerfield C, Junque C, Tolosa E, Salgado-Pineda P, Gomez-Anson B, Marti MJ, et al. Structural brain changes in Parkinson disease with dementia: a voxel-based morphometry study. Arch Neurol 2005; 62: 281–5.

Tolosa E, Wenning G, Poewe W. The diagnosis of Parkinson's disease. Lancet Neurol 2006; 5: 75–86.

Vaillancourt DE, Spraker MB, Prodoehl J, Abraham I, Corcos DM, Zhou XJ, et al. High-resolution diffusion tensor imaging in the substantia nigra of de novo Parkinson disease. Neurology 2009; 72: 1378–84.

Wattendorf E, Welge-Lussen A, Fiedler K, Bilecen D, Wolfensberger M, Fuhr P, et al. Olfactory impairment predicts brain atrophy in Parkinson's disease. J Neurosci 2009; 29: 15410–3.

Yoshikawa K, Nakata Y, Yamada K, Nakagawa M. Early pathological changes in the parkinsonian brain demonstrated by diffusion tensor MRI. J Neurol Neurosurg Psychiatry 2004; 75: 481–4.

Zecca L, Youdim MB, Riederer P, Connor JR, Crichton RR. Iron, brain aging and neurodegenerative disorders. Nat Rev Neurosci 2004; 5: 863–73.